A&A 582, A34 (2015)
DOI: 10.1051/0004-6361/201526110

Astronomy & Astrophysics

RETRACTED ARTICLE: *r*-process nucleosynthesis in the MHD+neutrino-heated collapsar jet

K. Nakamura[1], T. Kajino[2,3], G. J. Mathews[4,2], S. Sato[2,⋆], and S. Harikae[2,⋆⋆]

[1] Waseda University, Ohkubo 3-4-1, Shinjuku, 169-8555 Tokyo, Japan
e-mail: nakamura.ko@heap.phys.waseda.ac.jp
[2] National Astronomical Observatory of Japan, Osawa 2-21-1, Mitaka, 181-8588 Tokyo, Japan
e-mail: kajino@nao.ac.jp
[3] Department of Astronomy, Graduate School of Science, The University of Tokyo, 7-3-1 Hongo, Bunkyo-ku, 113-0033 Tokyo, Japan
[4] Center for Astrophysics, Department of Physics, University of Notre Dame, Notre Dame, IN 46556, USA
e-mail: gmathews@nd.edu

Received 17 March 2015 / Accepted 23 May 2015

ABSTRACT

It has been proposed that the collapsar scenario for long-duration gamma ray bursts is a possible astrophysical site for *r*-process nucleosynthesis. Here we present *r*-process nucleosynthesis calculations based upon a model for a MHD+neutrino-heated collapsar jet. We utilize a relativistic magnetohydrodynamic model that includes ray-tracing neutrino transport to describe the development of the black hole accretion disk and the neutrino heating of the funnel region above the black hole. The late time evolution of the collapsar jet is then evolved using axisymmetric special relativistic hydrodynamics. We employ representative test particles to follow the trajectories in density, temperature, entropy, and electron fraction for material flowing from the accretion disk into the jet until they are several thousand km above the black hole. The evolution of nuclear abundances from nucleons to heavy nuclei for ejected test particle trajectories was solved in a large nuclear reaction network as temperatures fall from 9×10^9 to 3×10^8 K. We show that an *r*-process-like abundance distribution forms in material ejected in the collapsar jet. The possibility for a signature of collapsar *r*-process material to be found in metal-poor stars is discussed.

Key words. gamma-ray burst: general – stars: black holes – accretion, accretion disks – magnetohydrodynamics (MHD) – stars: abundances – stars: massive

1. Introduction

Nucleosynthesis by a process of rapid neutron-capture (the *r*-process) accounts for about a half of the abundance of nuclei heavier than iron. However, even after many years of study, the neutron-rich astrophysical site for *r*-process nucleosynthesis has not yet been definitively identified. There are, however, three important observational clues. One is that the abundance pattern of heavy neutron-capture elements in the range $Z \geq 56$ ($130 \leq A \leq 190$) in old metal poor stars in the Galactic halo (such as CS22892-052) is nearly identical to that of the solar-system *r*-process abundance distribution. This universality suggests a unique *r*-process mechanism that was active very early on in the history of the Galaxy. This early appearance argues for events associated with massive stars (Mathews et al. 1992; Argast et al. 2000). Another important clue comes from the large dispersion (Sneden et al. 2003; Honda et al. 2006) in *r*-process elements like [Eu/Fe] vs. [Fe/H] compared to other elements in the most metal-poor stars. This strongly argues (Ishimaru et al. 2005; Lan et al. 2010) that the *r*-process is a rare event only occasionally enriching local regions of the interstellar medium compared to other elements in the early ejecta from stars. A third clue is the fact that the *r*-process abundances in the solar system only comprise a mass fraction of about $X_r \sim 10^{-7}$. For a Galaxy mass of $10^{11}\ M_\odot$, this corresponds to only about $10^4\ M_\odot$ of *r*-process material in the Galaxy. For an average core-collapse supernova rate of $\sim 10^{-2}$ yr^{-1} over 10^{10} years, then an average ejected mass of only $\sim 10^{-4}\ M_\odot$ of *r*-process material per supernova has occurred over the history of the Galaxy (Mathews & Cowan 1990).

Within this context a number of astrophysical candidate sites have been proposed that may satisfy the energetic and high neutron density requirements for the *r*-process (Mathews & Cowan 1990; Shibagaki et al. 2015). Among these, the most popular involve: the neutrino-driven wind from core-collapse supernovae (Woosley et al. 1994), neutron star mergers (Freiburghaus et al. 1999), and magnetohydrodynamic jets from supernovae (Nishimura et al. 2006).

None of these possible sites, however, is without problems. For example, the original neutrino-driven wind model (Woosley et al. 1994) successfully reproduced the observed *r*-process abundance distribution up to the third ($A \approx 195$) *r*-process peak. However, that calculation was based upon the supernova models of Mayle & Wilson (1988), that generated very high entropy per baryon ($s/k_B = 400$) and neutron-rich material. However, such high entropy and high neutron fraction has been difficult to achieve in more recent core-collapse simulations, e.g. Fischer et al. (2012). Also, in the neutron star merger model it is not clear whether the mergers can occur early enough to account

⋆ *Present address*: SMBC Nikko Securities Inc., 3-3-1 Marunouchi, Chiyoda-ku, 100-8325 Tokyo, Japan
⋆⋆ *Present address*: Quants Research Department, Financial Engineering Division, Mitsubishi UFJ Morgan Stanley Securities Co., Ltd.

for the early enrichment of *r*-process material in the Galaxy (Mathews & Cowan 1990; Argast et al. 2000). Although the supernova magnetohydrodynamic (MHD) jet scenario can reproduce *r*-process abundances (Nishimura et al. 2006; Winteler et al. 2012; Shibagaki et al. 2015), the fraction of supernovae that experience such events is highly uncertain.

On the other hand, there has been some interest (Fujimoto et al. 2006, 2007, 2008; Surman et al. 2008; Ono et al. 2012; Nakamura et al. 2013) in the possibility of *r*-process nucleosynthesis in the relativistic jets associated with the collapsar (failed supernova) model for gamma-ray bursts. See Nakamura et al. (2013) for a recent review. Collapsars are a favored model for the formation of observed long-duration gamma-ray busts (GRBs). In the collapsar model (Woosley 1993; Paczynski 1998; MacFadyen & Woosley 1999, 2001; Popham et al. 1999; Aloy et al. 2000; Zhang et al. 2003) the central core of a massive star collapses to a black hole. Angular momentum in the progenitor star, however, leads to the formation of a heated accretion disk around the nascent black hole. Magnetic field amplification and heating from the pair annihilation of thermally generated neutrinos emanating from this accretion disk (Vieyro et al. 2013) can then launch material in a polar funnel region leading to an outflow of matter within a relativistic jet along the polar axis.

A large volume of work has explored the formation of such collapsars (e.g. Takiwaki et al. 2004, 2009; Kotake et al. 2004; Sawai et al. 2004; Obergaulinger et al. 2006; Suwa et al. 2007; Burrows et al. 2007; Taylor et al. 2011; see also references in Kotake et al. 2006), and the development of the associated relativistic jets (e.g. MacFadyen & Woosley 1999, 2001; Popham et al. 1999; Aloy et al. 2000; Zhang et al. 2003; Proga & Begelman 2003; Hawley & Krolik 2006; Mizuno et al. 2007; Fujimoto et al. 2006; McKinney & Narayan 2007; Komissarov & McKinney 2007; Nagataki et al. 2007; Barkov & Komissarov 2008; Nagakura et al. 2011).

For the present work we make use results from Harikae et al. (2009) in which slowly rotating collapsar models were studied using an axisymmetric special relativistic magnetohydrodynamics (MHD) code. Subsequently, Harikae et al. (2010) developed a method (but did not apply it) to compute the detailed neutrino-pair heating by ray-tracing neutrino transport. In the present work we apply this ray-tracing method to explore whether the collapsar model is indeed capable of generating the high entropy per baryon and neutron-rich material required for an *r*-process in a high-Lorentz-factor jet heated via neutrino-pair annihilation.

The computational intensity of evolving relativistic axisymmetric MHD with full neutrino transport, however, limited the study reported here using the method of Harikae et al. (2009, 2010) for the time evolution of the jet to a duration of only ~200 ms. Although this time is sufficiently long for the development of a relativistic jet, this timescale is too short for a study of *r*-process nucleosynthesis in the jet. In the present work, therefore, we have extended those hydrodynamic studies of material in the heated jet along with the associated nucleosynthesis out to the much later times and lower temperatures associated with the *r*-process. We evolve representative trajectories and their associated physical variables for material ejected in the outflow. We then present numerical results of extended *r*-process nucleosynthesis network calculations within this heated jet outflow. We show that this environment can indeed produce an *r*-process-like abundance distribution. We note, however, that a proper treatment of the jet would require higher resolution than the current approach affords. Therefore, the present work provides a lower limit on the yield of *r*-process nuclei. This is because the production of the heaviest nuclei may be dominated by small regions of ejecta with very high entropy. Nevertheless, the present application is sufficient to demonstrate that an *r*-process-like abundance pattern indeed forms in the collapsar jet. Hence, this study should motivate future studies with higher resolution.

2. Collapsar model

When a rotating massive star (35–40 $M_\odot$) collapses and produces a black hole, an accretion disk is formed. Jets ejected from the polar region above the black hole could then be a source for observed long-duration GRBs (Woosley 1993). The inner region of the accretion disk near the black hole becomes a neutron-rich environment due to electron captures on protons. So this is a possible *r*-process site (Fujimoto et al. 2007; Ono et al. 2012). Details of the explosion, however, involve several steps: 1) first, there is the initial collapse of the progenitor massive star leading to the formation of the accretion disk and black hole; 2) as the accretion disk heats up and the magnetic fields are amplified, a funnel region above the pole of the black hole is heated by neutrinos and magnetic fields; 3) this leads to the launch of a relativistic jet which is eventually dominated by the propagation of a hydrodynamic shock through the outer layers of the progenitor. In this paper we are primarily concerned with this final phase. In particular, we study the epoch during which the jet cools from $T_9 = 9$ to $T_9 = 0.3$ (where T_9 is the temperature in units of 10^9 K). In this temperature range nuclei can combine to form *r*-process material. We briefly summarize here the previous steps which are partially detailed in Harikae et al. (2009, 2010).

2.1. Progenitor collapse and accretion disk formation

The calculations of Harikae et al. (2009) were based upon a relativistic axisymmetric MHD code (Takiwaki et al. 2009) to describe the collapse of rotating magnetic massive stars. They employed an initial model from the spherical data set (temperature, density, initial energy and electron fraction) from the 35OC model of Woosley & Heger (2006) as a progenitor of the collapsar. The collapse of the rotating massive star was evolved for more than ~10 s without heating by neutrino-pair annihilation, but including thermal neutrino production and cooling in the accretion disk. After about 9 s a stable accretion disk was formed and the total neutrino luminosity exceeded 10^{52} erg s^{-1}.

2.2. MHD driven outflow

As a stable accretion disk develops, an MHD driven outward flow can launch from the funnel region above the pole of the nascent black hole. If the magnetic field is strong enough, the magnetic field (and associated magnetic pressure) in the accretion disk is amplified up to as much as 10^{16} G. This leads to a magnetic tower explosion above the polar region and relativistic outflow. Depending upon the angular momentum, when the magnetic field strength is weaker, the magnetic tower at first stalls, but then the magnetic twisting of turbulent inflowing material in the accretion disk again transports magnetic pressure to the polar region and the stalled magnetic shock is reheated so that the outward flow continues.

Based upon their simulations, Harikae et al. (2009) identified the optimum conditions to generate a high-entropy MHD driven jet. It was found that a relatively slowly rotating model with initial specific angular momentum $j = 1.5 j_{\rm iso}$ (where $j_{\rm iso}$ is the specific angular momentum of material in the innermost stable circular orbit) produced the highest neutrino luminosity

in the accretion disk. Not surprisingly, the best magnetic outflow in the jet was produced with the highest initial magnetic fields corresponding to $B = 10^{10}$ G for the core of the progenitor. We use these conditions as the best case for analyzing *r*-process nucleosynthesis in the outflowing material.

2.3. Neutrino-heating in the funnel region

It was noted in Harikae et al. (2009), however, that the simple MHD driven outflow can only reach mildly relativistic speeds and weak explosion energies. Those calculations, however, did not include heating in the funnel region by $\nu - \bar{\nu}$ pair annihilation from the 10^{52} erg s^{-1} of neutrinos emitted from the hot accretion disk. Moreover, Harikae et al. (2009) evaluated whether the dynamical time scale $\tau_{\rm dyn}$ for material to be ejected in the funnel regions was longer than the heating time scale $\tau_{\rm heat}$ by neutrino-pair annihilation. They argued that material for which $\tau_{\rm dyn}/\tau_{\rm heat} > 1$ could gain enough thermal energy by neutrino-pair annihilation to drive the jet to highly relativistic escape velocities from the gravitational field. They found that after about 9.1 s this condition was satisfied. Thus, in the calculation reported here, the jet evolution calculation was restarted from the results of Harikae et al. (2009) after 9.1 s. The neutrino-induced heating in the funnel region above the nascent black hole was added to the simulation by employing a special relativistic ray-trace method as described in Harikae et al. (2010). We note that the simulation of the disk and subsequent jet formation was limited to 50 angles and 400 radial zones in a dynamic grid. Although this resolution is adequate to determine the bulk properties of the jet, a detailed understanding of the structure of the jet would require much higher resolution. That, however, is beyond the scope of the present work. Nevertheless, the present resolution is adequate for our purposes, i.e. to develop a relativistic jet and establish whether an *r*-process like abundance distribution can emerge.

In the method of Harikae et al. (2010) only radiation emanating from the neutrino sphere of the accretion disk is considered, and a Fermi-Dirac form for the neutrino distribution function is assumed. The computational time is reduced significantly by only updating the neutrino-pair annihilation rate after 50 MHD time steps. Also, the calculation avoids following uninteresting neutrino trajectories by employing an algorithm that omits trajectories that are emitted toward the inside of the neutrino sphere, stop in the optically thick equatorial region, or become lost within the black-hole horizon. However, even with these simplifications, the added computational complexity of the detailed neutrino heating calculation limited the duration of the jet evolution computed in the present work to only ~200 ms from the time that the stable accretion disk and evacuated funnel region was formed.

Even this short time frame, however, was adequate to establish that a relativistic jet had indeed formed. Figure 1 shows the density, entropy per baryon, and velocity structures of the jet from the present calculation based upon the MHD+neutrino-heating simulation described in Harikae et al. (2010). One can see from these figures that by the end of this portion of the simulation, the outflowing material is contained in a narrowly focused jet that has already reached Lorentz factors of ~2–3. Note, in particular that along the jet axis the entropy per baryon can achieve very high values ($S/k \sim 10^4$, where k is the Boltzmann constant) while the density varies from 10 to 10^4 g cm^{-3} along the jet. These are ideal *r*-process initial conditions as discussed further below.

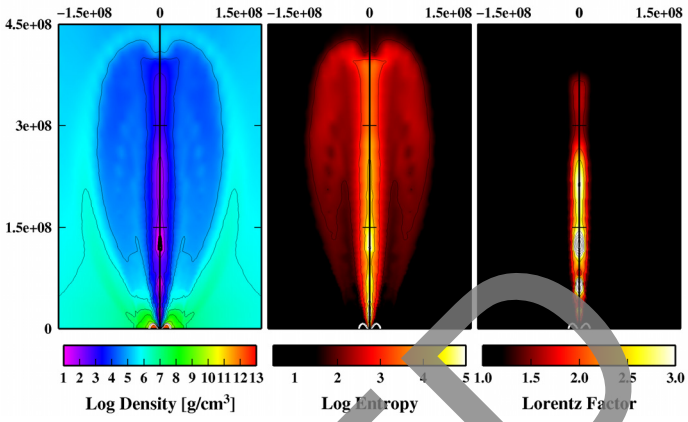

Fig. 1. Profiles in the *xy* plane of density, entropy per baryon and Lorentz factor for the jet at the end of the MHD+neutrino-heating simulation for $x = -1.5 \times 10^{-8}$ to $+1.5 \times 10^{8}$ cm and $y = 0$ to 4.5×10^{8} cm.

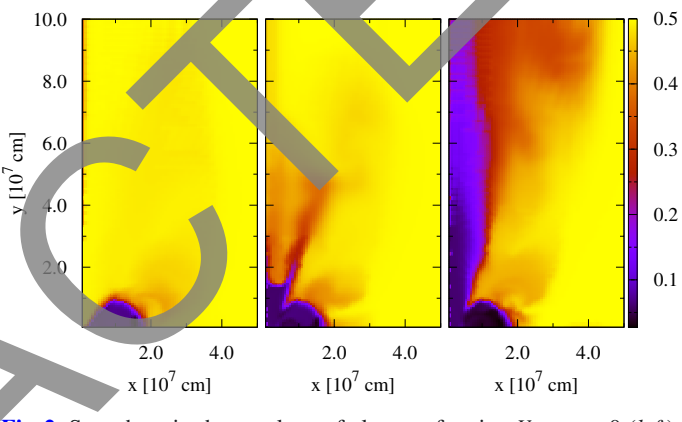

Fig. 2. Snapshots in the *xy* plane of electron fraction $Y_{\rm e}$ at $t = 0$ (*left*), 40 ms (*middle*) and 80 ms (*right*). Note the low $Y_{\rm e}$ material in the accretion disk and the central jet.

We would also like to point out that Fig. 2 shows contours of electron fraction $Y_{\rm e}$ for material flowing into and out of the accretion disk and jet. This is very important for the development of *r*-process nucleosynthesis. Material with initially high electron fraction ($Y_{\rm e} \sim 0.5$) is neutronized as it is incorporated into the high density accretion disk. Hence, the accretion disk has $Y_{\rm e} \sim 0.1$. As this material flows out of the inner accretion disk into the jet it remains at low $Y_{\rm e}$ so that material flowing within the neutrino heated jet is very neutron rich. As noted below, this is because the timescale for transport to high distances from the jet is short compared to the timescale for weak interactions to increase $Y_{\rm e}$. Material moving more slowly away from the central polar axis, however, is converted to higher $Y_{\rm e}$ by neutrino interactions as shown in Fig. 2. All together, this leads to a distribution of *r*-process environments with different initial entropy per baryon and $Y_{\rm e}$ that contribute the final mass distribution. These different trajectories are roughly characterized by the angle away from the polar axis as discussed below.

More insight can be gained from the snapshots of the jet development shown in Fig. 3. The right side of each figure has white arrows superimposed upon it corresponding to the outward flow of the jet. The top panels show an extended view of the initial conditions for the present network nucleosynthesis calculations. These figures demonstrate the hydrodynamic conditions when the accretion disk is in a stationary state (at about 9.1 s after the onset of gravitational collapse) as determined in Harikae (2010). At this point MHD heating has already produced a mild

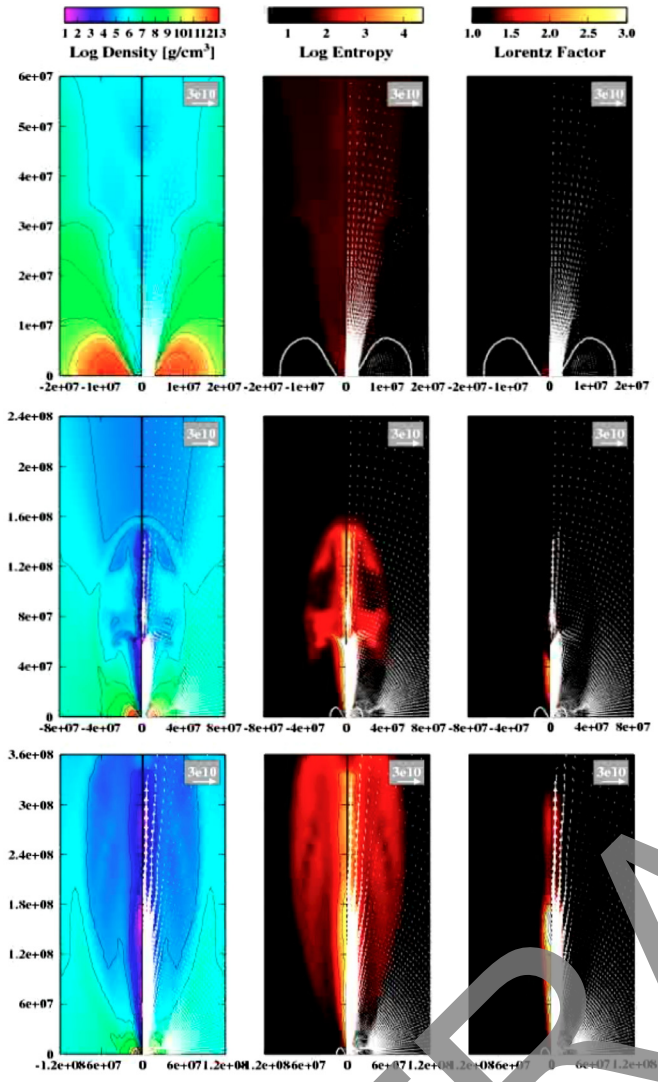

Fig. 3. Snapshots in the *xy* plane of density, entropy per baryon and Lorentz factor during the development of the jet at $t = 0$ (*top*), 60 ms (*middle*) and 200 ms (*lower*). Note the change of scale from 6×10^7 cm at $t = 0$ to 2.4×10^8 cm at $t = 60$ ms to 3.6×10^8 cm for the *bottom figure* at $t = 200$ ms. Note also the Rayleigh-Taylor instability when the jet encounters the inward flowing material above the funnel region at $y \approx 10^8$ cm and t = 60 ms.

jet and an evacuated funnel region above the black hole out to about 10^7 cm. The middle panel in Fig. 3 shows the formation of the jet after pair annihilation from neutrino heating is added to this simulation. Note the development of a Rayleigh-Taylor instability at a distance of about 10^8 cm above the black hole. This results as the jet encounters inflowing material above the funnel region. This causes outward flowing material in the jet to temporarily halt its adiabatic cooling as it circulates backward into the low density high-temperature material behind the jet. The material then continues outward smoothly once it moves beyond this discontinuity. This behavior will be particularly apparent in the tracer particle trajectories described in the next section.

2.4. Tracer particles

In order to follow the evolution of mass elements in the collapse and ejecta we have employed 20 000 tracer particles moving

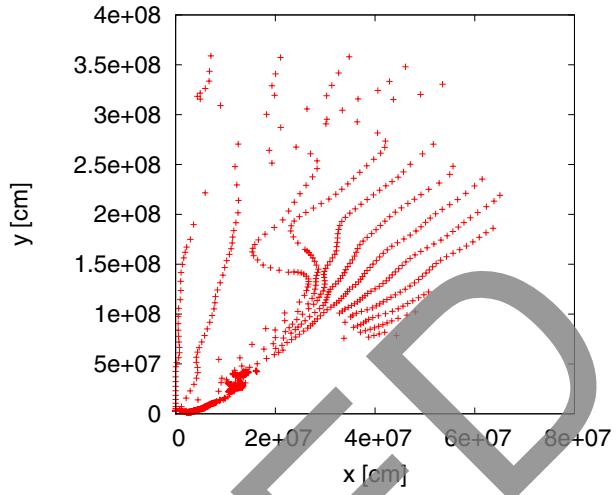

Fig. 4. A snapshot at $t = 200$ ms of the distribution of the 1289 tracer particles that are ultimately incorporated into the jet and ejected as the heated outflow.

with the material. These were distributed as one particle per zone in the resolution of the MHD+neutrino-heating simulation, i.e. 50 angles and 400 radial zones. We note that nothing would be gained by adding more tracer particles, as this number corresponds to 1 particle per zone. On the other hand, one expects that to properly resolve the jet and the ejected material a higher resolution and more test particles would be desired. The *r*-process nucleosynthesis calculations here should, therefore, be considered as lower limits to the possible nucleosynthesis that may be dominated by small regions at very high entropy per baryon to produce the third *r*-process peak. We return to this point below.

The test particles so distributed, were then analyzed to determine which of the particles would eventually be incorporated into the outflow, i.e. $\tau_{\rm dyn}/\tau_{\rm heat} > 1$. The nucleosynthesis evolution was then studied for those outflowing mass elements.

Of the 20 000 tracer particles, 1289 of them were determined to be participating in the MHD+neutrino-heated jet. Since the entire particle history was desired, these 1289 particles were then post-processed to reconstruct their history of escape from the accretion disk and into the jet. Figure 4 shows the distribution of those 1289 particles as the neutrino-heated jet begins to develop. Already by this time particles closest to the polar region have been ejected to the edge of the computational grid at 3.6×10^8 cm from the black hole. Note that the finger-like distribution of these tracer particles away from the accretion disk is due to the initial distribution along 50 angles and 400 radial zones.

The physical conditions during the *r*-process for the ejected particles can be approximately characterized by the angle of emission with respect to the jet axis. Figure 5 shows the reconstructed history of the location of eight outflowing mass elements ejected at different angles. These trajectories begin at about the same radial distance from the source but at increasing angles in increments of 5° from the polar axis. The particles begin their trajectories at a distance of a few $\times 10^6$ cm just inside the inner accretion disk around the black hole. At this point the material begins as low $Y_{\rm e}$ material flowing into the jet from the high density, low $Y_{\rm e}$ inner accretion disk. One can see that, once launched into the jet, they quickly rise to $\sim 10^8$ cm from the source.

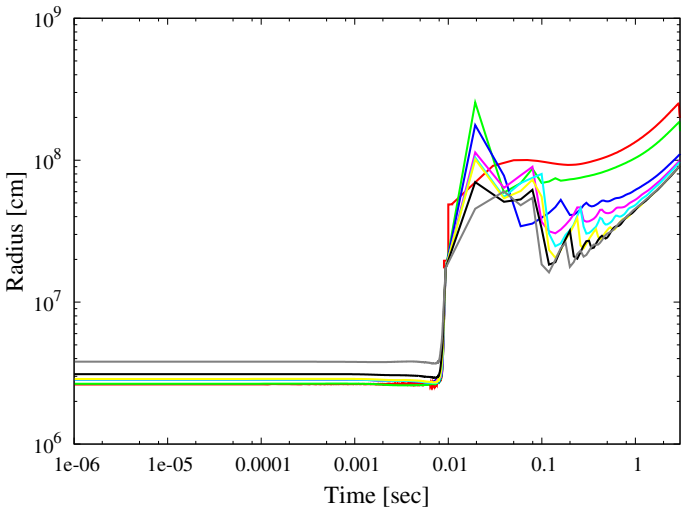

Fig. 5. Distance vs. time for representative trajectories ejected in the jet. Red, green, blue, pink, sky blue, yellow, orange and gray indicate representative test particles for 8 trajectories which originate at about the same distance from the source but eject at increasing angles from the polar axis from 2.5 to 37.5 degrees in increments of 5 degrees.

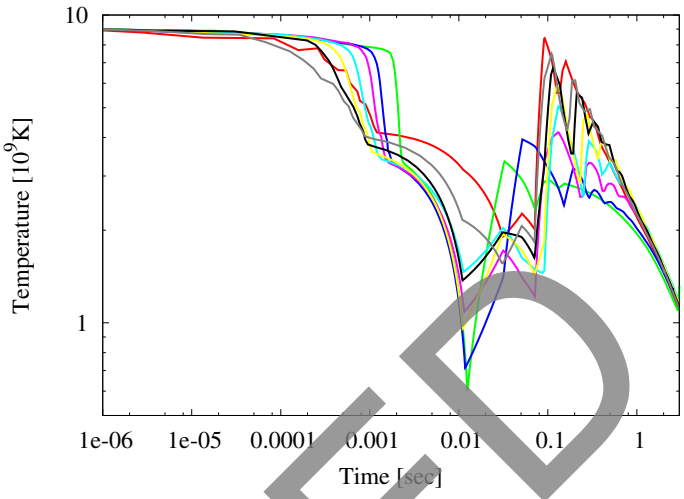

Fig. 6. The same as Fig. 5, but for temperature vs. time.

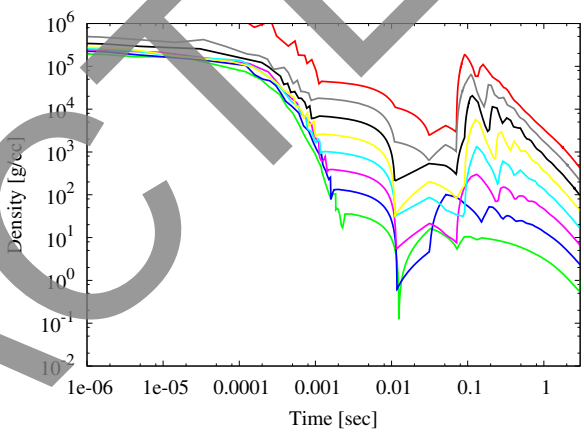

Fig. 7. The same as those for Fig. 5, but for density vs. time.

2.5. Hydrodynamic flow far from the source

The temperature of material as the jet reached the outer edge of the grid at the end of the MHD+neutrino-heating simulation was $T_9 \sim 9$. At this temperature all nuclei are in nuclear statistical equilibrium corresponding to photodissociation into free nucleons and alpha particles. An extension of the simulation of the outflow and cooling in the outer region of the jet was, therefore, necessary to evolve the cooling into the temperature range appropriate to *r*-process nucleosynthesis ($5 > T_9 > 0.3$). On the other hand, by the end of the MHD+neutrino-heating simulation, the heated material in the jet was sufficiently distant from the accretion disk to no longer be affected significantly by neutrino scattering or the magnetic field. Rather, the jet outflow becomes an outgoing hydrodynamic shock dominated by the ram pressure of the ejected material.

In the present simulation, therefore, we could supplement the model of MHD+neutrino-heating with an outer relativistic axisymmetric hydrodynamic simulation to follow the jet as it propagated through the outer layers of the progenitor star. Within that flow we evolved the nucleosynthesis network for the 1289 ejected test particles as the temperature and density decreased. The final abundance distribution was then obtained from a mass-weighted sum of the outflowing trajectories.

We followed the time evolution of temperature, density, velocity and electron fraction for test particles of outflowing material in a computational grid that extended far beyond that of the original collapsar model of Harikae et al. (2009, 2010). The evolution of the chemical and isotopic composition associated with each test particle trajectory was calculated in an extended nuclear reaction network (Otsuki et al. 2000; Terasawa et al. 2001; Sasaqui et al. 2005). The network includes all reactions relevant to the synthesis of nuclides from nucleons to actinides. The hydrodynamics was evolved in an axisymmetric two-dimensional simulation that takes into account the effects of special relativistic fluid motion. It is based upon the piecewise parabolic method (PPM, Mignone et al. 2005) which enabled the simulation to run for long times and out to large distances.

As initial conditions we incorporated the final distribution of physical variables given by the output of the MHD+neutrino-heating simulation. The collapsing stellar envelope corresponding to the 35OC model of Woosley & Heger (2006) was attached over the core region as was adopted in Harikae et al. (2009). For the jet evolution studies, the central black hole of mass 2.02 $M_\odot$ was replaced with a point mass. As noted above, the simulation did not include the transport and pair-annihilation of neutrinos beyond the 0.2 s of the MHD+neutrino-heating calculation. This is because once the jet is launched away from the inner funnel region, the MHD, neutrino-pair annihilation heating, and neutrino nucleon interactions could be neglected as shown below.

The time evolution of temperature, density, and electron fraction Y_e from incorporation into the MHD+neutrino-pair heated collapsar jet through the end of the *r*-process nucleosynthesis at $T_9 \sim 1$ is shown in Figs. 6–8, respectively, for the eight representative trajectories of Fig. 5. In all of these trajectories the development of the Rayleigh-Taylor instability at $t \approx 0.1$ s into the simulation is readily apparent in the reversal of the distance, temperature, densities, and Y_e that occur at that time. At this point all test flows are temporarily compressed and the temperature and density become high. After passing through the instability, however, the temperature and density begin to decrease again. In the *r*-process calculation discussed below, the final heavy element abundances are all produced after the passage of this instability.

The slightly different evolution for trajectories at large angles with respect to the polar axis is apparent in these figures. The red curves correspond to particles most closely aligned with

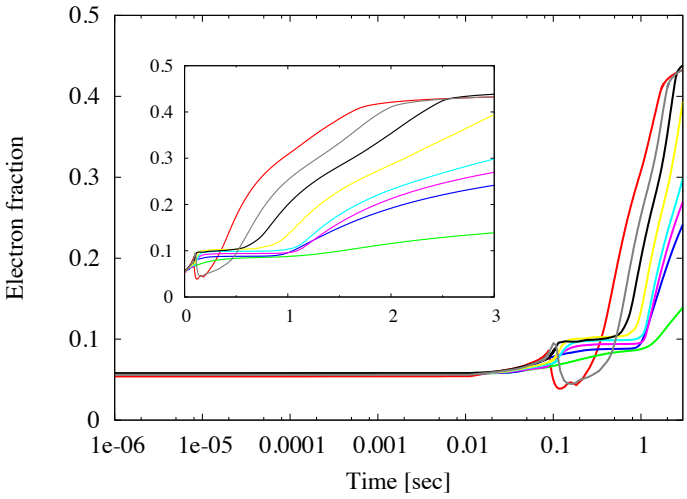

Fig. 8. The same as those for Fig. 5, but for electron fraction Y_e vs. time. *Insert* shows the linear growth in Y_e.

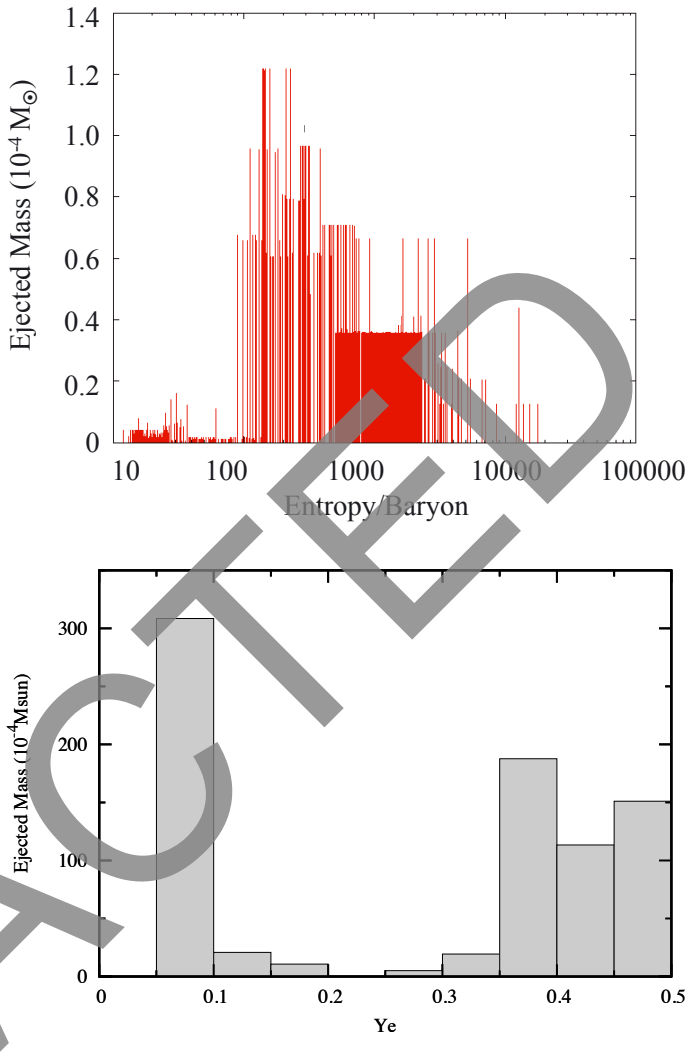

Fig. 9. Ejected mass distribution for the 1289 ejected test particles. The *upper panel* shows the ejected mass as a function of the initial entropy per baryon. The *lower panel* shows ejected mass as a function of the final Y_e.

the axis. Because of this they are less affected by the Rayleigh-Taylor instability as is evidenced in Figs. 5 and 6. The sudden drop in temperature for $t \sim 0.001$ s is due to a rapid cooling as the trajectory moves away from the high-temperature evacuated central region of the jet. This also accounts for the early drop in density at $t \sim 0.001$ s in Fig. 7 as particles are incorporated into the high temperature low density central region of the jet. Note also that material moving at larger angles with respect to the polar axis show a more exaggerated effect from the Rayleigh-Taylor down turn. They are also more affected by subsequent neutrino interactions and hence rise to higher Y_e.

A few comments are in order concerning the evolution of Y_e. The initial low values of $Y_e < 0.1$ are typical of material flowing out of the high density inner accretion disk as noted in Harikae et al (2010). As material is launched from the highly neutronized accretion disk, interactions with the neutrino luminosity of 10^{53} erg s^{-1} might be expected to reset the Y_e to higher values due to $n + \bar{\nu}_e \rightarrow p + e^+$. However, as can be seen in Fig. 5, material is quickly transported to >1000 km from the black hole and the neutrino source. At >1000 km from the black hole the neutrino luminosity decreases from 10^{53} to 10^{47} erg cm^{-2} s^{-1}. For ~MeV neutrinos then the neutrino flux is $\sim 10^{41}$ cm^{-2} s^{-1}. For a typical neutrino interaction cross section at ~1 MeV of 10^{-43} cm^{-2}, the capture rate per particle is then 10^{-2} s^{-1}. Hence, the timescale for neutrino interactions (~100 s at 10^8 cm, 1 s at 10^7 cm) is much longer than the timescale for material to escape in the jet (~0.02 s). It is also much longer than the timescale for the r-process ~2 s at 10^8 cm. Thus, at the radius in question the effect of neutrino interactions is negligible and its effect on Y_e can be ignored in the present calculation. This is consistent with the low Y_e in the jet apparent in Fig. 2.

We also note, that the evolution of Y_e and entropy per baryon in this simulation is a bit different than that of the jet studies of Fujimoto et al. (2006, 2007, 2008), and Ono et al. (2012). This ultimately can be traced to their treatment of the neutrino heating and their assumption of simple adiabatic expansion in the jet at late times for the r-process. This is in contrast to the hydrodynamic evolution modeled here. In our model the expansion and thermodynamic evolution are determined by the dynamics of the outward flowing jet shock. In their paradigm, it was found that neutron-rich matter having Y_e values of around 0.2 provides a successful r-process within a rather mild ($S/k \lesssim 100$) entropy environment. For our model, however, the low entropy per baryon material tends to occur away from the relativistic jet and includes relatively high ($Y_e \sim 0.45$) material. As such, in our simulation the low entropy per baryon material does not produce r-process nuclides beyond the $A \sim 130$ r-process peak.

If the trajectories have higher entropy per baryon, their densities and Y_e are generally low and they correspond to relativistic jets that are formed near the polar axis. The electron fraction is low due to the neutrino interactions near the black hole. Near the black hole central engine, material in the jet is at relatively low density and the trajectories have temperatures of $T_9 > 9$. At such high temperatures nuclear statistical equilibrium (NSE) is obtained. In NSE, the material is mainly composed of free neutrons, protons and α-particles. As the temperature decreases down to $T_9 < 5$ the material falls out of NSE and the chemical composition of the material is calculated using a nuclear reaction network.

3. *r*-process nucleosynthesis

3.1. Distribution of physical conditions

The upper and lower panels in Fig. 9 show the ejected mass as a function of entropy per baryon (upper) and final Y_e (lower panel)

for the 1289 ejected trajectories in the jet. We found that trajectories emitted close to the polar axis have relatively high speed, high entropy per baryon ($S/k \geq 1000$), and the lowest Y_e (cf. Fig. 2). Hence, these trajectories can produce heavy elements up to and beyond the $A = 195$ *r*-process abundance peak. On the other hand, a significant fraction of the ejected mass involves trajectories emitted at angles away from the polar axis with relatively lower entropy per baryon ($100 \leq S/k \leq 1000$) and higher Y_e. These trajectories only produce light elements up to the $A = 130$ *r*-process peak. In total 0.082 $M_\odot$ of *r*-process material was ejected with the outflow in our simulation.

3.2. Nuclear reaction network

The β-decay half-lives, fission probabilities and (n,γ), (γ,n) reaction rates are important input for the *r*-process abundance calculation in the outflow. Whenever available, the experimental data and reaction rates have been used in the nuclear reaction network. Our nuclear reaction network code (Otsuki et al. 2000; Terasawa et al. 2001; Sasaqui et al. 2005) is able to calculate nucleosynthesis from NSE, the α-process, the α-rich freeze-out, the *r*-process and β-decay. This network code includes about 5000 nuclei. The calculation starts from free neutrons, protons and electrons in NSE at high temperature. We halt the network calculation when the temperature drops below $T_9 \leq 0.3$, or when the abundance of a nuclide becomes vanishingly small ($\leq 10^{-50}$).

4. Results

Figure 10 shows the final weighted isotopic abundance distribution for all 1289 trajectories emitted in the jet. This is compared with solar-system *r*-process abundances of Käppeler et al. (1989; red dots), and also examples of tracer-particle trajectories with different entropy per baryon corresponding to low ($S/k = 25$), intermediate ($S/k = 100$), and high ($S/k = 1000$). Here, we can see that this collapsar simulation produces elements up to the $A = 195$ *r*-process peak and that the abundance distribution in the region $140 < A < 180$ is approximately reproduced. The elemental abundances with $140 < A < 180$ between the two *r*-process peaks is referred to at the *universality* region because numerous observations of metal-poor halo stars (Sneden et al. 2003, 2008; Honda et al. 2006, 2007; Roederer & Lawler 2012) have demonstrated that the abundances in this region well match the solar-system *r*-process abundances. It is, therefore, crucial for any *r*-process model to reproduce this universality region.

We found that trajectories with very high entropy per baryon (~1000) can produce heavy elements up to the third *r*-process abundance peak and even beyond to the actinides. On the other hand, trajectories with relatively low entropy per baryon (~100) only produce light elements up to the 2nd *r*-process peak as is evident in Fig. 10.

It is of interest to contrast this finding with the generic *r*-process conditions as studied, for example, in Hoffman et al. (1997). In that paper the conditions necessary to form up to the third *r*-process peak were deduced numerically. These were then found to be well reproduced by the following analytic relation derived in that paper:

$$\frac{S}{k} \approx 10^3 \left\{ \frac{1-2Y_{e,i}}{[0.33/(Y_{e,i}-0.17)]^2 - (1/2Y_{e,i})^2} \left(\frac{t_{exp}}{s}\right) \right\}^{1/3}, \quad (1)$$

where $Y_{e,i}$ is the initial electron fraction presumed to remain constant, and the expansion time is taken as $t_{exp} = 1.28\tau_{dyn}$, where

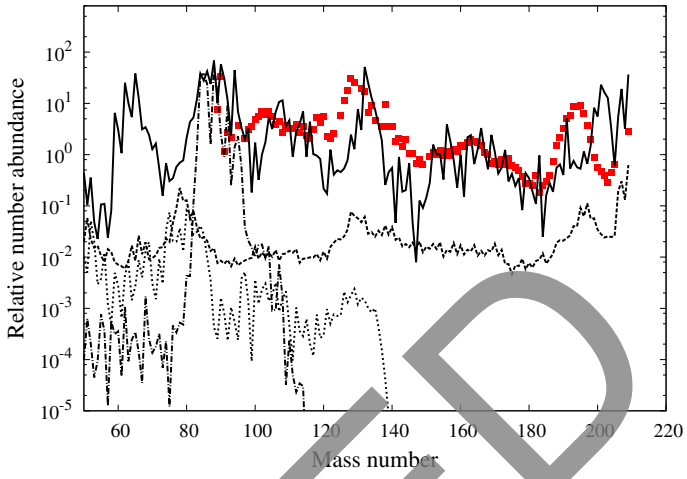

Fig. 10. Summed mass-weighted abundance distribution (solid line) for the 1289 ejected tracer particles. These are compared with the solar system *r*-process abundances (points) of Käppeler et al. (1989) and normalized at ^{153}Eu. Also shown are arbitrarily normalized abundances of elements synthesized in individual trajectories with high entropy $S/k = 1000$ (dashed), intermediate entropy $S/k = 100$ (dotted), and low entropy $S/k = 25$ (dash-dotted).

the dynamical time scale is assumed to be represented by an exponential evolution of temperature with time,

$$T_9(t) \approx T_9(0)\exp(-t/\tau_{dyn}). \quad (2)$$

Although, most of the temperature evolution in Fig. 6 is not well represented by an exponential, the high entropy material leading to the third *r*-process peak can be approximated by a dynamical timescale of $\tau_{dyn} \approx 3$ s when *r*-process nucleosynthesis begins after $t > 1$ s. The expansion timescale is then $t_{exp} \approx 4$ s. From the insert to Fig. 8 it is apparent that the electron fraction is not constant, but grows linearly. Nevertheless, if we adopt a median value from the insert in Fig. 8 of $Y_{e,i} \approx 0.25$ for for $t > 1$ s when *r*-process nucleosynthesis begins, then for an expansion time of $t_{exp} = 4$ s, one would need an entropy of $S/k > 500$ from Eq. (1). Hence, although we are dealing with very high entropy and low Y_e compared, for example, to a neutrino-driven wind scenario (Woosley et al. 1994). We find that very high entropy ejecta are required to produce the third *r*-process peak. This can be ultimately traced to the fact that we are dealing with an expansion timescale in the jet that is orders of magnitude longer than that of a typical neutrino driven wind, e.g. $t_{exp} = 4$ s in the jet vs. 0.005 s in some wind scenarios (Hoffman et al. 1997).

Although this distribution is certainly *r*-process like, there are some detailed differences with the solar-system *r*-process abundances that can be traced to the physics of the relativistic jet simulation. One difference is that the calculated isotopes with $A \sim 120, 145, 185$ are significantly underproduced. Another is that the 2nd ($A \sim 130$) and the third ($A \sim 195$) peaks are slightly shifted to higher mass numbers ($A \sim 132$ and $A \sim 200$). There is also a larger odd-even effect exhibited in the model calculations than in the solar-system abundances. The underproduction near $A = 120, 145, 185$ is a common feature in dynamic *r*-process calculations (e.g. Woosley et al. 1994; Nishimura et al. 2012; Shibagaki et al. 2015). These features could be an artifact of an overestimated strength of the shell closure at $N = 82$, effects of beta-delayed neutron emission, or underestimated β-decay rates near $N = 82$ and 126 (Nishimura et al. 2011, 2012; Suzuki et al. 2012). Nevertheless, we caution that as noted above, the structure of the outflow in the jet is not

well resolved in these simulations. Hence, the abundance yields in the heaviest *r*-process nuclides should be considered as lower limits to the *r*-process yields because the yields may be enhanced by small unresolved regions at higher entropy and low Y_e. Given this caveat, however, we can speculate on other possible physical mechanisms for the differences between the calculated *r*-process yields and the solar-system abundances.

The shifting of the peaks to higher mass number in the calculation can result if the neutron density at freezeout is too low or the temperature is too high. This causes the *r*-process path to run closer to stability thereby shifting the mass number at which the *r*-process path reaches the $N = 82$ and 126 neutron closed shells to higher mass numbers. This is also consistent with the large odd-even effect that can be smoothed if there are residual neutron captures after freezeout, but remains large if the neutron abundance diminishes rapidly.

This shifting of *r*-process peaks may suggest that the jet does not cool fast enough in our model, or that the neutron density in the jet diminishes too rapidly. We note that if this shift of the *r*-process to higher mass numbers is a general characteristic of the collapsar jet model, then one might hope to find such a unique abundance distribution in a small fraction of low metallicity halo stars whose abundance distribution might reflect the yields of a single collapsar event (Mathews et al. 1992).

Regarding the possibility of detecting the ejected material from collapsar events, we note that our model ejects about 0.1 $M_\odot$ of *r*-process material in the jet. This is a large amount of material for an *r*-process event and could be evident as an enhancement in *r*-process elements in the next generation of stars contaminated by such an event. On the other hand, such events would only be expected to constitute a small fraction of the total number of events producing the *r*-process.

Observationally, collapsars are expected (Mathews et al. 2014) to only result from a very small fraction (0.04%) of stars in the range of $25\ M_\odot < m < 125\ M_\odot$. On the other hand, the core collapse supernova rate involves progenitor stars in the range of $10\ M_\odot < m < 25\ M_\odot$. Then the ratio of collapsar events to core-collapse supernova events is given by ratio of the integrated initial mass functions $\phi(m) \propto m^{-2.3}$ times the small fraction of massive stars that lead to a collapsar. This would correspond to only about 1 collapsar per 10^4 core collapse supernovae.

On the other hand, the production of normal heavy *r*-process events does probably not occur in all supernovae (Mathews & Cowan 1990; Ishimaru et al. 2005). It is currently believed that the neutrino driven wind scenario (Woosley et al. 1994) can only produce light elements below the first *r*-process peak (Shibagaki et al. 2015). The production of heavy *r*-process elements probably requires a MHD jet that occurs in about ~3% of core collapse supernovae (Shibagaki et al. 2015). Alternatively, the early *r*-process events may have been produced by neutron-star mergers. The relative rates of collapsar *r*-process events to the total number of *r*-process events will therefore depend upon whether the early *r*-process ejecta is associated with supernova jets, or neutron-star mergers.

There is a great deal of uncertainty in estimating the rates of neutron-star mergers or MHD jets relative to core-collapse supernovae. However, if we adopt the current galactic rates as a rough guide, the galactic neutron star merger rate is estimated to be 80^{+200}_{-70} Myr^{-1} (Kalogera et al. 2004), while the galactic supernova rate is inferred to be $1.9 \pm 1.1 \times 10^4$ Myr^{-1} (Dhiel et al. 2006). All together this suggests that the *r*-process merger events occur at a rate of about 1 per 20 supernovae, while MHD jets will occur at a rate of about 1 per 30 supernovae, and collapsar events only occur in 1 out of 10^4 supernovae.

Now, assuming similar mass yields from all three events we can equate these relative rates to the fraction of *r*-enhanced stars that might be attributable to each process. If the *r*-process occurs in either MHD jets or neutron-star mergers, then roughly only about 1 out of 400 *r*-enhanced stars would show this collapsar element distribution. That being the case it may be a while before evidence of this abundance distribution could be found. Of the approximately 600 currently know metal poor halo stars (Beers 2012; Frebel & Norris 2015; SAGA Database[1]) accumulated over decades of study, about 100 show an enhancement in *r*-process elements (defined as $r-I$ and $r-II$ stars; Beers & Christlieb 2005; Beers 2012). Hence, one would desire a sample size of of several times more *r*-process enhanced metal-poor stars before such a detection might be likely. Indeed, such statistics are possible in the near future (Beers & Christlieb 2005; Beers 2012).

5. Conclusion

In summary, we have investigated *r*-process nucleosynthesis in the neutrino-heated collapsar jet. We extended the MHD+neutrino-heated collapsar calculations as described in Harikae et al. (2009, 2010) with an axisymmetric hydrodynamic model so that we could evolve test mass elements to much later times and greater distance from the accretion disk. The important result of interest from the present work is that an *r*-process-like abundance distribution forms in the outflow. In detail, however, the *r*-process peaks appear at slightly higher mass numbers and there is a pronounced odd-even effect in the mass distribution. This suggests that there may be a unique signature of such collapsar-induced heavy-element nucleosynthesis observable in metal-poor halo stars. Clearly, more detailed studies of this collapsar model for *r*-process nucleosynthesis are warranted.

In our model the ejected mass of *r*-process material (~0.1 $M_\odot$) per collapsar event is a bit high. Nevertheless, this is a rare event compared to normal supernovae. Therefore, such events probably contribute insignificantly to the total solar *r*-process abundances. Nevertheless, the possible influence of such events on the abundance distribution in *r*-enhanced metal poor halo stars needs to be explored in a separate galactic chemical evolution model such as that of that of Ishimaru et al. (2005) or Lan et al. (2010).

Acknowledgements. We would like to express our gratitude to Dr. N. Nishimura for fruitful discussions. This work was supported in part by Grants-in-Aid for Scientific Research of JSPS (20244035, 24244036). Scientific Research on Innovative Area of MEXT (26105517, 24340060), JSPS Core-to-Core Program EFES. Numerical computations were carried out in part on the general common use computer system at the Center for Computational Astrophysics (CfCA) of the National Astronomical Observatory of Japan. Work also supported by the US National Science Foundation under Grant No. PHY-0855082, and the US Department of Energy under Nuclear Theory Grant DE-FG02-95-ER40934, and Grants-in-Aid for JSPS Fellows (21.6817).

References

Aloy, M. A., Müller, E., Ibàñez, J. M., Martí, J. M., & MacFadyen, A. 2000, ApJ, 531, L119
Argast, D., Samland, M., Gerhard, O. E., & Thielemann, F.-K. 2000, ApJ, 356, 873
Barkov, M. V., & Komissarov, S. S. 2008, MNRAS, 385, L28
Beers, T. C. 2012, PoS(NIC XII)056
Beers, T. C., & Christlieb, N. 2005, ARA&A, 43, 531
Burrows, A., Dessart, L., Livne, E., Ott, C. D., & Murphy, J. 2007, ApJ, 664, 416

[1] http://saga.sci.hokudai.ac.jp/Retrieval/db.cgi

Dhiel, R., Halloin, H., Kretschmer, K., et al. 2006, Nature, 439, 45
Käppeler, F., Beer, H., & Wisshak, K. 1989, Rep. Prog. Phys., 52, 945
Fischer, T., Martínez-Pinedo, G., Hempel, M., & Liebendörfer, M. 2012, Phys. Rev. D, 85, 083003
Frebel, A., & Norris, J. E. 2015, ARA&A, 53, 631
Freiburghaus, C., Rosswog, S., & Thielemann, F.-K. 1999, ApJ, 525, L121
Fujimoto, S.-I., Kotake, K., Yamada, S., Hashimoto, M.-A., & Sato, K. 2006, ApJ, 644, 1040
Fujimoto, S.-I., Hashimoto, M.-A., Kotake, K., & Yamada, S. 2007, ApJ, 656, 382
Fujimoto, S.-I., Nishimura, N., & Hashimoto, M.-A. 2008, ApJ, 680, 1350
Harikae, S., Takiwaki, T., & Kotake, K. 2009, ApJ, 704, 354
Harikae, S., Kotake, K., & Takiwaki, T. 2010, ApJ, 713, 304
Hawley, J. F., & Krolik, J. H. 2006, ApJ, 641, 103
Hoffman, R. D., Woosley, S. E., & Qian, Y.-Z. 1997, ApJ, 482, 951
Honda, S., Aoki, W., Ishimaru, Y., Wanajo, S., & Ryan, S. G. 2006, ApJ, 643, 1180
Honda, S., Aoki, W., Ishimaru, Y., & Wanajo, S. 2007, ApJ, 666, 1189
Ishimaru, Y., Wanajo, S., Aoki, W., Ryan, S. G., & Prantzos, N. 2005, Nucl. Phys. A, 758, 603
Kalogera, V., Kim, C., Lorimer, D. R., et al. 2004, ApJ, 614, L137
Komissarov, S. S., & McKinney, J. C. 2007, MNRAS, 377, L49
Kotake, K., Yamada, S., & Sato, K. 2003, ApJ, 595, 304
Kotake, K., Sato, K., & Takahashi, K. 2006, Rep. Prog. Phys., 69, 971
Lan, N. Q., Giang, N. T. , Mathews, G. J., & Saleh, L. 2010, Comm. Phys., 20, 23
MacFadyen, A. I., & Woosley, S. E. 1999, ApJ, 524, 262
MacFadyen, A. I., Woosley, S. E., & Heger, A. 2001, ApJ, 550, 410
Mathews, G. J., & Cowan, J. J. 1990, Nature, 345, 491
Mathews, G. J., Bazan, G., & Cowan, J. J. 1992, ApJ, 391, 719
Mathews, G. J., Hidaka, J., Kajino, T., & Suzuki, J. 2014, ApJ, 790, 115
Mayle, R. W., & Wilson, J. R. 1988, ApJ, 334, 909
McKinney, J. C., & Narayan, R. 2007, MNRAS, 375, 513
Meyer, B. S., Mathews, G. J., Howard, W. M., Woosley, S. E., & Hoffman, R. D. 1992, ApJ, 399, 656
Mignone, A., Plewa, T., & Bodo, G. 2005, ApJ, 160, 199
Mizuno, Y., Hardee, P., & Nishikawa, K.-I. 2007, ApJ, 662, 835
Nagakura, H., Ito, H., Kiuchi, K., & Yamada, S. 2011, ApJ, 731, 80
Nagataki, S., Takahashi, R., Mizuta, A., & Takiwaki, T. 2007, ApJ, 659, 512
Nakamura, K., Kajino, T., Mathews, G. J., Sato, S., & Harikae, S. 2013, Int. J. Mod. Phys. E, 22, 133022
Nishimura, S., Kotake, K., Hashimoto, M.-A., et al. 2006, ApJ, 642, 410
Nishimura, S., Li, Z., Watanabe, H., et al. 2011, Phys. Rev. Lett., 106, 052502
Nishimura, N., Kajino, T., Mathews, G. J., Nishimura, S., & Suzuki, T. 2012, Phys. Rev. C, 85, 048801
Obergaulinger, M., Aloy, M. A., Dimmelmeier, H., & Müller, E. 2006, A&A, 457, 209
Ono, M., Hashimoto, M., Fujimoto, S., Kotake, K., & Yamada, S. 2012, Prog. Th. Phys., 128, 741
Otsuki, K., Tagoshi, H., Kajino, T., Wanajo, S.-Y. et al. 2000, ApJ, 533, 424
Paczynski, B. 1998, ApJ, 494, L45
Popham, R., Woosley, S. E., & Fryer, C. 1999, ApJ, 518, 356
Proga, D., & Begelman, M. C. 2003, ApJ, 592, 767
Roederer, I. U., & Lawler, J. 2012, ApJ, 750, 76
Sasaqui, T., Kajino, T., & Balantekin, A. B. 2005, ApJ, 634, 534
Sawai, H., Kotake, K., & Yamada, S. 2005, ApJ, 631, 446
Shibagaki, S., Kajino, T., Mathews, G. J., et al. 2015, ArXiv e-prints [arXiv:1505.02257]
Sneden, C., Cowan, John J., Lawler, James E., et al. 2003, ApJ, 591, 936
Sneden, C., Cowan, J. J., & Gallino, R. 2008, ARA&A, 46, 241
Surman, R., Beun, J., McLaughlin, G. C., Kane, S., Hix, W. R., et al. 2008, J. Phys. G, 35, 014059
Suwa, Y., Takiwaki, T., Kotake, K., & Sato, K. 2007, PASJ, 59, 771
Suzuki, T., Yoshida, T., Kajino, T., & Otsuka, T. 2012, Phys. Rev. C, 85, 015802
Takiwaki, T., Kotake, K., Nagataki, S., & Sato, K. 2004, ApJ, 616, 1086
Takiwaki, T., Kotake, K., & Sato, K. 2009, ApJ, 691, 1360
Taylor, P. A., Miller, J. C., & Podsiadlowski, Ph. 2011, MNRAS, 410, 2385
Terasawa, M., Sumiyoshi, K., Kajino, T., Mathews, G. J., & Tanihata, I. 2001, ApJ, 562, 470
Vieyro, F. L., Romero, G. E., & Peres, O. L. G. 2013, A&A, 558, A142
Winteler, C., Käppeli, R., Perego, A., et al. 2012, ApJ, 750, L22
Woosley, S. E. 1993, ApJ, 405, 273
Woosley, S. E., & Heger, A. 2006, ApJ, 537, 810
Woosley, S. E., Wilson, J. R., Mathews, G. J., Hoffman, R. D., & Meyer, B. S. 1994, ApJ, 433, 229
Zhang, W., Woosley, S. E., & MacFadyen, A. I. 2003, ApJ, 586, 356